Bulletin of Electrical Engineering and Informatics
Vol. 13, No. 2, April 2024, pp. 832~844
ISSN: 2302-9285, DOI: 10.11591/eei.v13i2.6088

Maximum allowable hp rating of 3-phase induction motor fed through a stand-alone constant V/f controlled DFIG via RSC

Mohamed Sharawy[1], Adel A. Shaltout[2], Omar El-Sayed Mohammed Youssef[1], Mahmoud A. Al-Ahmar[1], Naser Abdel-Rahim[3], Tole Sutikno[4,5]
[1]Department of Electrical Engineering, Faculty of Engineering at Shoubra, Benha University, Cairo, Egypt
[2]Department of Electrical Power and Machines, Faculty of Engineering, Cairo University, Cairo, Egypt
[3]Department of Electrical Engineering, Faculty of Engineering and Technology, Future University in Egypt, New Cairo, Egypt
[4]Master Program of Electrical Engineering, Faculty of Industrial Technology, Universitas Ahmad Dahlan, Yogyakarta, Indonesia
[5]Embedded System and Power Electronics Research Group, Yogyakarta, Indonesia

Article Info

Article history:

Received Feb 25, 2023
Revised Sep 11, 2023
Accepted Dec 17, 2023

Keywords:

Loading capacity limits
Induction motor starting
Mathematical model
Stand-alone doubly fed induction generator
V/f control

ABSTRACT

This paper presents a scheme to start three-phase induction motors (IMs) directly connected to terminals of constant V/f controlled doubly fed induction generator (DFIG) through the rotor side converter (RSC). The proposed control is achieved by controlling the output voltage and frequency of stand-alone DFIG via controlling an injected voltage into the rotor circuit through the RSC. The control scheme provides a search for maximum rating of the three-phase IM which can be supplied from a DFIG. The search technique is based on using a simplified mathematical model to find the capability limits of the RSC and DFIG. It is found that these parameters depend on the stator frequency and rotor slip. Therefore, an investigation is performed to find the lowest frequency and the corresponding allowable maximum rating for the IM to be safely started. A typical example is provided in the paper for a 15 kW DFIG. It is shown that this generator could supply a three-phase IM with a maximum rating of 1-hp if it operated at nominal outputs, voltage and frequency, during start-up period. While, using the proposed technique, the same generator could start-up a three-phase IM with maximum power rating of 7.25 hp.

Corresponding Author:

Mohamed Sharawy
Department of Electrical Engineering, Faculty of Engineering at Shoubra, Benha University
108 Shobra, Borham, Elsahel, Cairo Governorate, Cairo, Egypt
Email: mohamed.anwer@feng.bu.edu.eg

1. INTRODUCTION

Stand-alone wind energy conversion systems employing doubly fed induction generators (DFIG) have become a suitable choice for feeding low power consumers in remote areas [1]–[16]. DFIG can produce a constant outputs, terminal voltage and frequency (VF), using field-oriented control (FOC) when supplying isolated loads regardless of the loading conditions and generator operating speed [1], [17], [18]. In remote area applications, where the DFIG is used as a power source, dynamic loads such as induction motors (IM) are used in farm irrigation pumps [19]. As it is known, the directly connected IM to the power source draws large starting current (6 times the nominal value) with low power factor, causing a voltage dip during start-up period [20]. This voltage dip reduces the motor starting torque [21]. Hence, the performance and analysis of the motor fed from DFIG is needed.

Much research has been carried out on different aspects of the static loads and on the dynamic performance of the DFIG [1], [22]. However, the dynamic loads had little attention especially the impact of

the start-up current on the operation of the DFIG. Naidu and Singh [23], Singh and Sharma [24] have proposed control algorisms for the load-side-converter (LSC) and the rotor-side-converter (RSC) during start-up time of directly connected a three-phase IM. RSC is controlled to maintain the DFIG output VF constant at nominal values. Moreover, controlling the LSC contributes to operating DFIG stator terminals at unity power factor. Both previous control methods have not treated the motor starting current. In addition, testing of those control strategies has been carried out on an IM with directly connected start-up method and very low power rating according to the rating of DFIG. Hence, a larger rating of IM has not been used.

Sharawy *et al*. [18] has proposed a new method when the IM is directly connected to the DFIG. The output VF of the DFIG is firstly reduced to certain value before connection of the IM while maintaining the V/f ratio constant. Once the IM is connected across the DFIG output terminals, the output VF are started to increase gradually until reaches to their nominal value. The control method is implemented by applying constant V/f control beside with FOC to the RSC. This procedure contributes to the reduction of motor starting current and makes it possible to start larger IMs rating with respect to the DFIG rating. Furthermore, the procedure mitigates the voltage sag which occurs during the starting period within allowable limit values [25] without oversizing the rating of DFIG or employing any special starters [18].

However, operating DFIG at lower values of output VF reduces its loading capacity limits as its capacity depends mainly on the value of stator voltage [26]–[28]. Also, in normal operation of DFIG, the slip range is limited to ± 30% from its nominal synchronous speed. But operating DFIG at low output frequency produces an increasing of the slip and slip power output from RSC to the DC-bus. Hence, at higher stator output power and low output frequency, the slip power may exceed the allowable limits of the RSC power rating. This has required oversizing RSC although the stator output power does not exceed the nominal power of DFIG when operating it at lower values of output VF. So, when DFIG is operated at inconstant stator output VF and feeds a motor load, it is important to determine the loading capacity limits of the DFIG to prevent an overload. Previous research [26]–[28] is implemented on the grid connected DFIG, which always operates at constant VF and does not deal with a DFIG operating at variable output VF or dynamic loads. With inconstant VF, the RSC active power capability, slip range and steady state stability limitations according to those operating conditions should be taken into consideration.

In this paper, maximum allowable hp rating of a three-phase motor can be started when using stand-alone DFIG is determined. The system under study, see Figure 1, consists of a wind turbine (WT) drives a DFIG through a gear box (GB). The DFIG is supplied from the rotor using battery and RSC. The three-phase IM is directly connected across DFIG stator terminals through a circuit breaker (CB) and drives an irrigation pump. A C-filter is connected to stator terminals to reduce the DFIG output voltage harmonics.

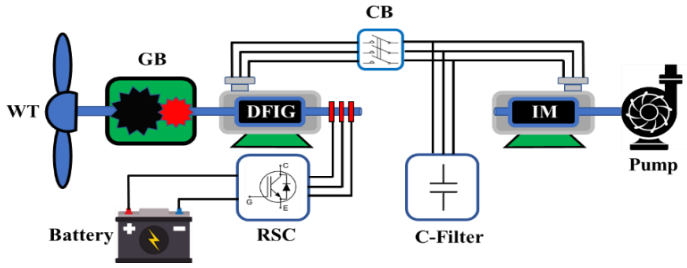

Figure 1. Proposed system scheme

A simplified steady state mathematical model is presented to evaluate the loading capacity limits of DFIG at steady state. The DFIG loading capacity limits and the RSC power rating are determined at different output VF of the stator while maintaining V/f ratio constant. For varying the stator output VF, FOC control method is applied. The maximum allowable hp rating of a three-phase IM is determined when the DFIG stator is operated at nominal output VF. Then, the maximum allowable hp rating is obtained when the DFIG stator is operated at variable output VF while maintaining V/f ratio fixed. A typical example of a 15 kW generator is considered. The system is simulated using MATLAB/Simulink and the simulation results show the capacity limits of DFIG when operated at different output VF of stator while feeding a three-phase IM.

2. STEADY STATE MATHEMATICAL REPRESENTATION OF DFIG

The voltages and currents relations for the DFIG according to the traditional per phase equivalent circuit at steady state of DFIG, referred to stator side, shown in Figure 2(a), are depicted as (1)-(4) [26]–[28]:

$$\vec{E}_m = \vec{V}_s + \vec{I}_s(R_s + jX_{Ls}) \quad (1)$$

$$\vec{E}_m = jX_m\vec{I}_m \quad (2)$$

$$\vec{I}_m = -(\vec{I}_s + \vec{I}_r) \quad (3)$$

$$\vec{V}_r/s = \vec{E}_m - \vec{I}_r(R_r/s + jX_{Lr}) \quad (4)$$

Where $\overrightarrow{V_s}$ is the phasor of stator output voltage with frequency f_s; $\overrightarrow{V_r}$ is the phasor of the supplied rotor voltage; $\overrightarrow{I_s}$, $\vec{I}_m$ and $\overrightarrow{I_r}$ are the stator, magnetizing, and rotor current phasors respectively; R_r and R_s are the effective resistance or rotor and stator winding respectively; X_{Lr} and X_{Ls} are the leakage reactance of the rotor and stator winding respectively; X_m and $\vec{E}_m$ are the magnetizing reactance and the induced internal voltage phasor respectively; and *s* is the slip of the rotor and obtained from the relation:

$$s = \frac{n_s - n}{n_s} \quad (5)$$

Where *n* and n_s are the rotor mechanical speed and DFIG synchronous speed at specified operating frequency respectively. Substituting (3) into (2) then:

$$\vec{E}_m = \vec{E}_{os} - jX_m\vec{I}_s \quad (6)$$

$$\vec{E}_{os} = -jX_m\vec{I}_r \quad (7)$$

Substituting (6) into (1) and (2), (3) into (4) gives:

$$\vec{E}_{os} = \vec{V}_s + \vec{I}_s(R_s + jX_s) \quad (8)$$

$$\vec{V}_r = \vec{I}_r[(-R_r - sX_m\frac{I_s}{I_r}sin(\theta_{Is} - \theta_{I_r})) + j(-sX_r + sX_m\frac{I_s}{I_r}cos(\theta_{Is} - \theta_{I_r}))] \quad (9)$$

Where X_r and X_s are the rotor and stator winding reactance respectively; $\vec{E}_{os}$ and δ are the generator induced voltage at no-load and the angle between $\vec{E}_{os}$ and $\overrightarrow{V_s}$ respectively; θ_{Is} and θ_{Ir} are the angle between $\overrightarrow{I_s}$ and $\overrightarrow{V_s}$ and between $\overrightarrow{I_r}$ and $\overrightarrow{V_s}$ respectively. If the stator current assumed to be lagged the stator output voltage with angle φ, then, (9) is rewritten as (10) and (11):

$$\vec{V}_r = -\vec{I}_r[(R_r + sX_m\frac{I_s}{I_r}cos(\varphi + \delta)) + j(sX_r - sX_m\frac{I_s}{I_r}sin(\varphi + \delta))] = -\vec{I}_r(R_{rt} + jX_{rt}) \quad (10)$$

$$V_r = I_r\sqrt{R_{rt}^2 + X_{rt}^2} \quad (11)$$

Where R_{rt} and X_{rt} are the total rotor equivalent resistance and reactance respectively; I_s and I_r are the rms of the stator and rotor currents respectively; and V_r is the rotor rms voltage. The simplified equivalent circuit presented in Figure 2(b) can be obtained from (8) and (10).

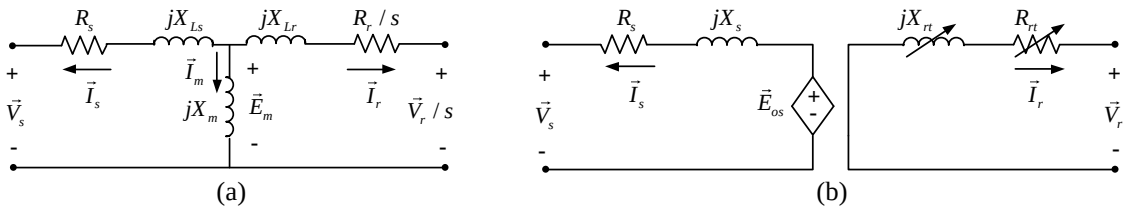

Figure 2. Equivalent circuit of a DFIG; (a) traditional equivalent circuit and (b) simplified equivalent circuit

As shown in Figure 2(b), the stator equivalent circuit representation side is like steady state stator equivalent circuit representation side of the synchronous generator. If resistance of stator winding is

neglected, then the DFIG phasor diagram for the equivalent circuit representation of the stator side is shown in Figure 3(a) [26]. The corresponding power phasor diagram can be deduced from Figure 3(a), by multiplying the axes by $3V_s/X_s$ as illustrated in Figure 3(b) [29].

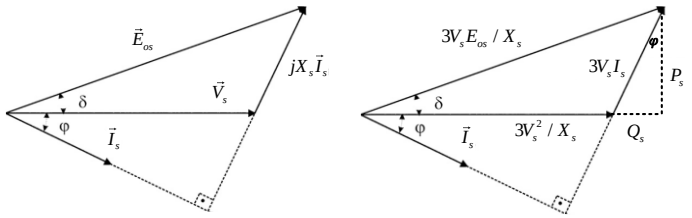

(a) (b)

Figure 3. DFIG (a) phasor diagram of the stator and (b) power phasor diagram

From Figures 2(a) and (b), apparent, active, and reactive power of the stator can be given as (12)-(14) [26]–[28]:

$$S_s = 3V_sI_s^* = P_s + jQ_s \quad (12)$$

$$P_s = \frac{3V_sE_{os}}{X_s} sin\,\delta \quad (13)$$

$$Q_s = \frac{3V_sE_{os}}{X_s} cos\,\delta - \frac{3V_s^2}{X_s} \quad (14)$$

Where V_s and E_{os} in rms values. If the rotor copper losses are neglected, then the apparent, active/reactive rotor power is expressed by [26]–[28]:

$$S_r = 3V_rI_r^* = P_r + jQ_r \quad (15)$$

$$P_r = -s\frac{3V_sE_{os}}{X_s} sin\,\delta \quad (16)$$

$$Q_r = -s[3I_r^2X_r + \frac{3V_sE_{os}}{X_s} cos\,\delta - \frac{3E_{os}^2}{X_s}] \quad (17)$$

3. LOADING CAPACITY LIMITS OF STAND-ALONE DFIG

In stand-alone wind energy conversion systems based on DFIG, the reactive power requirements of the loads are supplied through the LSC or the stator of DFIG. Generally, it is preferred to operate DFIG in case of stand-alone at unity power factor where the reactive power for the loads is supplied totally by the LSC [30]. In the proposed system, see Figure 1, the DFIG is only the source of the active/reactive power required by the loads. Hence, the active output power ability of the DFIG will be decreased to meet the loads reactive power requirements [20]. Wherefore, the loading capacity limits for the proposed system are mainly obtained by the capabilities of both DFIG and RSC. The next sections study the capacity limits of 15 kW DFIG [31] and the effect on the power swap between the RSC and DC-bus according to the variation of stator outputs VF, and slip.

3.1. DFIG loading capacity limits

DFIG loading capacity limits in steady state operation are deduced at the rotor and stator maximum permissible currents, nominal values [26], and at the rotor maximum permissible voltage [32]. For constant V/f operation, the constant of proportionality (c) is given by:

$$c = \frac{V_{sr}}{f_{sr}} \quad (18)$$

Where V_{sr} and f_{sr} are the nominal values of the DFIG stator output VF. For any given stator frequency (f_s) the voltage of the stator is expressed by:

$$V_s = cf_s \quad (19)$$

The loading capacity limits of DFIG can be calculated at any operating VF as in the next sections.

3.1.1. Stator current limit

This can be implemented by taking the stator winding copper losses into consideration [26]. Substituting (19) into (12), (12) can rewritten as (20):

$$P_s^2 + Q_s^2 = (3cf_sI_{sr})^2 \quad (20)$$

At certain operating frequency, (20) shows that the maximum, nominal value, the locus for the current of the stator in the *PQ*-plane could be drawn as origin centered circle of a radius equal to nominal apparent power of the stator.

3.1.2. Rotor current limit

This can be achieved by taking the rotor winding copper losses into consideration. The locus of maximum current of the rotor is determined by replacing the values of E_{os} and V_s in (13) and (14) by the values given in (7) and (19), then:

$$P_s = \frac{3cf_sL_mI_r}{L_s} sin\ \delta \quad (21)$$

$$Q_s = \frac{3cf_sL_mI_r}{L_s} cos\ \delta - \frac{3c^2f_s}{2\pi L_s} \quad (22)$$

In (21) and (22) show that the maximum, nominal, rotor current locus in the *PQ*-plane is presented as (23):

$$P_s^2 + (Q_s + \frac{3c^2f_s}{2\pi L_s})^2 = (\frac{3cf_sL_mI_r}{L_s})^2 \quad (23)$$

Also, (23) is an equation of a circle centered at $[-3c^2f_s/2\pi L_s, 0]$ and having a radius equal to $3cf_sL_mI_r/L_s$.

3.1.3. Steady state stability limit

As deduced in (21), at certain frequency output from the stator and constant current from the rotor, the active power output is directly proportional to the stator frequency f_s and sin (δ). The stability limit at steady-state in the *PQ*-plane is given by a vertical straight line at point [$-3c^2f_s/2\pi L_s$,0]. The shaded area in Figure 4(a) illustrates the resulting loading capacity limits of DFIG in pu at nominal stator frequency output, f_s=50 Hz, according to rotor, stator, and stability limits at steady state [33].

With variable frequency operation, (20) to (23) show that, in addition to the previously discussed operating limits, the loading capabilities are directly proportional to the stator frequency. Figure 4(b) shows the DFIG loading capacity limits in pu at f_s=10 Hz maintaining V/f ratio constant. Comparing Figure 4(a) with Figure 4(b), it can be observed that the DFIG loading capacity limits decrease as the operating frequency decreases.

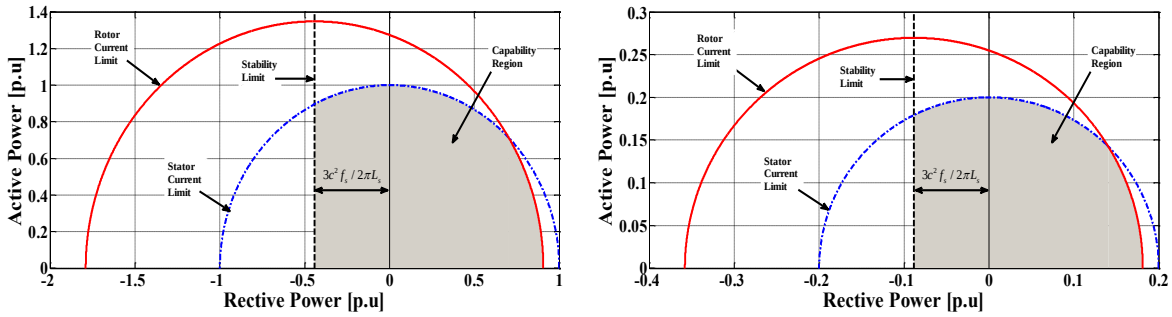

Figure 4. Loading capacity limits of DFIG; (a) at f_s=50 Hz and (b) at f_s=10 Hz

3.2. Ratings of the rotor side converter

The RSC is mainly used to regulate the DFIG stator VF outputs at desired magnitude regardless of wind speed variations and loading conditions. Also, it is used to govern the active/reactive power supplied from the stator and consumed by the loads. The limits of the LSC ratings are basically obtained from the

rotor current and voltage limits, consequently the nominal apparent power of the rotor. As explained earlier, the rotor current limit is restricted by the DFIG nominal value of 1.43 pu, however, the rotor voltage limit depends on the speed range of the rotor [32]. If the voltage drop due to the rotor resistance is neglected, (11) can be expressed as (24):

$$V_r = sf_s I_r \sqrt{(-2\pi L_m \frac{I_S}{I_r} cos(\varphi + \delta))^2 + (-2\pi L_r + 2\pi L_m \frac{I_S}{I_r} sin(\varphi + \delta))^2} \quad (24)$$

Referring to (24), at a certain stator and consequentially rotor current (see (7), (8), and Figure 2(b)), the square root magnitude is constant. Also, at a certain operating frequency, the desired voltage of the rotor, V_r, and the rotor slip, s, are directly proportional to each other. So, for the maximum permissible operating slip, the RSC must supply the voltage required by the rotor to obtain nominal VF outputs from the stator. For unity power factor operation of the DFIG, the maximum slip of 30% leads to the maximum rotor voltage of 0.3 pu [31].

To obtain the nominal reactive power from the DFIG, (24) shows that the rotor voltage reaches to maximum value of 0.4 pu. Higher slip values are possible when operating the DFIG at lower current values at the nominal frequency. In (24) also shows that even higher slip values are possible without exceeding the maximum rotor voltage if the stator voltage and frequency are reduced according to V/f constant law.

Figure 5(a) shows the changing of the rotor voltage against the rotor slip at nominal and zero output current of the stator with nominal frequency of the stator output, f_s=50 Hz. Also, it illustrates that limiting rotor voltage to a value of 0.4 pu, the DFIG rotor slip will have a maximum value of ± 0.3 pu at I_s=1 pu. However, at I_s=0 pu, the maximum slip can reach as high as ± 0.375 pu without exceeding the nominal rotor voltage. As a result, if the value of the stator current is somewhere between full-load and no-load, the rotor slip value will have a value between 0.3 and 0.375 pu. Figure 5(b) illustrates the changing of the rotor voltage against the rotor slip with nominal stator power factor and output current at stator frequencies, f_s=50 and 10 Hz. Also, it demonstrates that if the rotor voltage is limited to 0.4 pu according to RSC voltage capacity limit, the maximum operating rotor slip should be within ± 0.3 pu at 50 Hz and within ± 1.5 pu at 10 Hz.

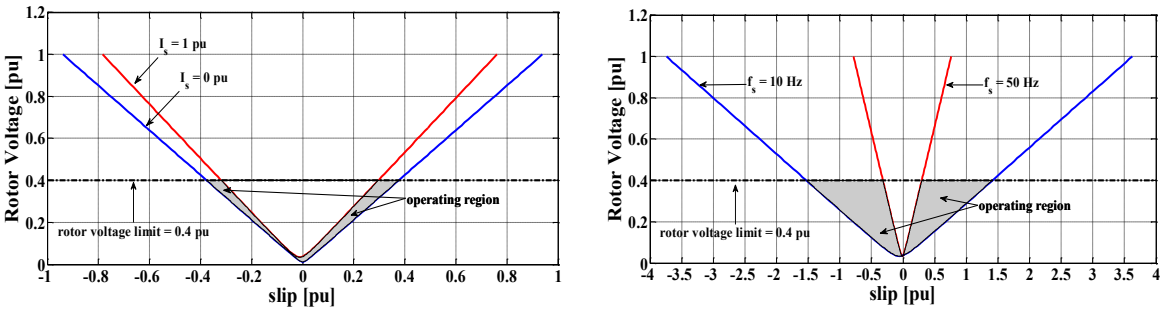

(a) (b)

Figure 5. Limit of the rotor voltage against the rotor slip; (a) at different output current of the stator and f_s=50 Hz and (b) at f_s=50 and 10 Hz

The RSC nominal apparent power obtained according to the rotor current and voltage limits which is usually about 30% of the generator nominal power [5], [34], [35]. Due to the load reactive power requirements from the DFIG, the power rating of RSC must be increased [36]. At rotor current and rotor voltage of 1.43 pu and 0.4 pu respectively, the nominal RSC power rating is nearly 60% of the generator power rating. Substituting (24) in (15), the rotor apparent power magnitude value is calculated as (25):

$$|S_r| = 3sf_s I_r^2 \sqrt{(-2\pi L_m \frac{I_S}{I_r} cos(\varphi + \delta))^2 + (-2\pi L_r + 2\pi L_m \frac{I_S}{I_r} sin(\varphi + \delta))^2} \quad (25)$$

In (25) illustrates that the rotor apparent power, RSC apparent power, depends on the stator outputs, the rotor current, and the rotor slip. For certain load current and stator output frequency, the required injected apparent power from the rotor and the rotor slip are directly proportional to each other. Figure 6 presents the rotor apparent power change versus slip of the rotor with stator frequencies output, f_s=50 and 10 Hz and at the nominal stator power factor and output current. The previous discussion reveals that special care must be taken to not go beyond the RSC limits in case of variable output VF with constant V/f ratio operation.

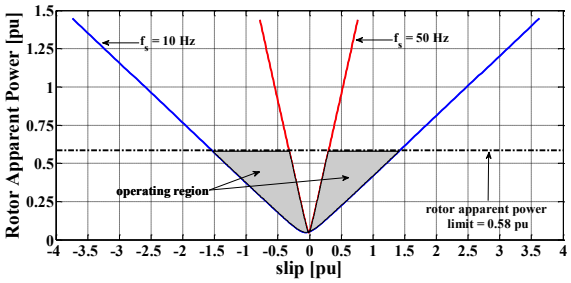

Figure 6. Slip versus apparent power of the rotor at f_s=50 and 10 Hz

4. DFIG VOLTAGE AND FREQUENCY CONTROL

The output VF control of the stand-alone DFIG can be obtained by adjusting the magnitude of currents and frequency of the rotor via the RSC from the reference values, V_s^*, and ω_s^* respectively. Figure 7(a) shows the proposed control method to choose the DFIG reference values of stator VF outputs by the help of control switch [18]. At position (a), the DFIG operates at nominal stator VF outputs. If the switch is moved to position (b), variable VF outputs operation while maintaining V/f ratio constant is obtained. At variable VF operation, DFIG controller produces stator VF outputs at low values while maintaining constant V/f ratio before and at the instant of load connection. After that, the DFIG output VF are gradually increased according to the ramp function, V/f ratio still constant, until they reach to their nominal values. The output frequency from the controller is limited to the DFIG nominal value using saturation block.

Then, the generated values of stator output VF references, V_s^*, ω_s^*, respectively are sent to the RSC controller. Figure 7(b) shows the indirect FOC algorithm scheme, based on direct voltage control, of RSC [37]. Controlling the RSC using FOC is implemented by using two independent control loops as follows:

a. Frequency control loop

Stator frequency is adjusted by defining a synchronously rotating reference frame related to the desired output frequency and imposing space vector of the stator-flux to be aligned with its *d*-axis. The alignment can be obtained by forcing i_{qr}^* so that [21], [37]:

$$i_{qr}{}^* = -\frac{L_s}{L_m} i_{qs} \tag{26}$$

Where L_s and L_m are the DFIG stator and mutual inductance, respectively.

b. Voltage control loop

The stator voltage control is achieved directly by regulating the magnitude of the rotor *d*-axis current component i_{dr}. The reference rotor *d*-axis current component i_{dr}^* is generated by processing the error of the voltage ϵ between the reference terminal voltage and estimated actual terminal voltage respectively, $\epsilon = V_s^* - V_s$, via PI regulator as seen in Figure 7(b). The per phase actual terminal voltage can be obtained as (27) [37]:

$$|V_s| = \sqrt{V_{qs}^2 + V_{ds}^2} \tag{27}$$

Then, the reference rotor currents *d* and *q* axis components (i_{dr}^* and i_{qr}^*) are compared with the actual rotor currents *d* and *q* axis components (i_{dr} and i_{qr}). Then, the current error is passed through the PI controller and compensators. Finally, the reference rotor voltage *d* and *q*-axis components (V_{dr}^*, and V_{qr}^*) are transformed to three-phase reference rotor voltages $V_{ar,br,cr}^*$ using inverse park transformation with slip angle (θ_{slip}) which can be calculated as (28) [21], [37]:

$$\theta_{slip} = \theta_s - \theta_r \tag{28}$$

The angle θ_s is obtained from the integration of the electrical angular frequency, ω_s rad/sec, however, θ_r is the electrical rotor angle and is obtained from speed sensor. The rotor reference voltages, $V_{ar,br,cr}^*$, are generated and used to estimate the modulating signals. Then they are compared to the fixed PWM frequency to obtain switching pulses to the RSC.

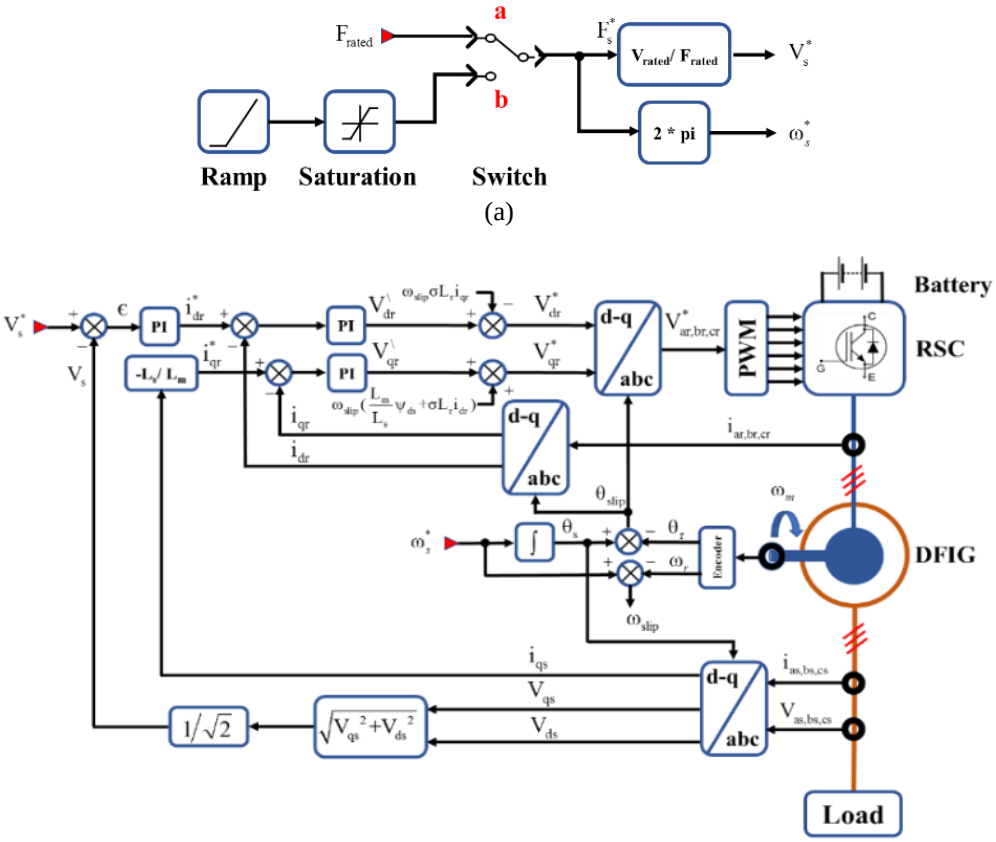

(a)

(b)

Figure 7. DFIG voltage and frequency control; (a) proposed control method of RSC and (b) indirect FOC of RSC

5. MAXIMUM ALLOWABLE HP RATING OF THREE-PHASE IM FED FROM DFIG

The starting current behavior, magnitude, and shape, mainly depends on the supply VF, class of the motor, motor hp rating, and the coupled mechanical load [21]. Also, it affects the transient behavior of the DFIG currents, voltages and power for both stator and rotor sides. When a stand-alone DFIG is used to supply a three-phase IM, the motor start-up current must be within the DFIG and RSC allowable capacity limits. The next sections present the maximum allowable hp rating of three-phase IM when the DFIG operated at nominal stator VF outputs as well as when it operated at V/f operation.

5.1. Nominal voltage and frequency operation

In the next steps, several IMs with different ratings of hp are connected individually to DFIG of 15 kW power rating so that the maximum allowable motor hp rating is determined when using the direct connected starting method. The DFIG stator VF outputs are maintained fixed at nominal magnitudes. The mechanical loads coupled with IMs have a speed-squared torque characteristic. The DFIG speed is first set at 1050 rpm (s=0.3 pu). The generator speed is held constant during starting and steady state. The DFIG is initially started at no load from t=0 to t=0.15 sec. with stator frequency equal to 50 Hz and corresponding stator voltage equal to 220 V per phase. The IM of 0.5 hp rating is directly connected to terminals of DFIG at t=0.15 sec. During start-up period, the rotor apparent power, the rotor voltage, the rotor current, and the stator current are recorded so that the RSC and DFIG power ratings do not pass the desired limits.

The pervious steps are repeated while the IM power rating is increased in each time until the maximum hp rating motor which can be started is obtained. The results illustrate that the DFIG can start-up an IM with hp rating of 1 hp at DFIG speed of 1050 rpm (s=0.3 pu). Figures 8(a) to (g) show the simulation results during start-up and steady state period of 1 hp IM [38]. As shown, the rotor voltage is close to its maximum limit of 0.4 pu while the reminder limits still below their maximum limits. Hence, the DFIG cannot start an IM above 1 hp as the rotor voltage will exceed its limits.

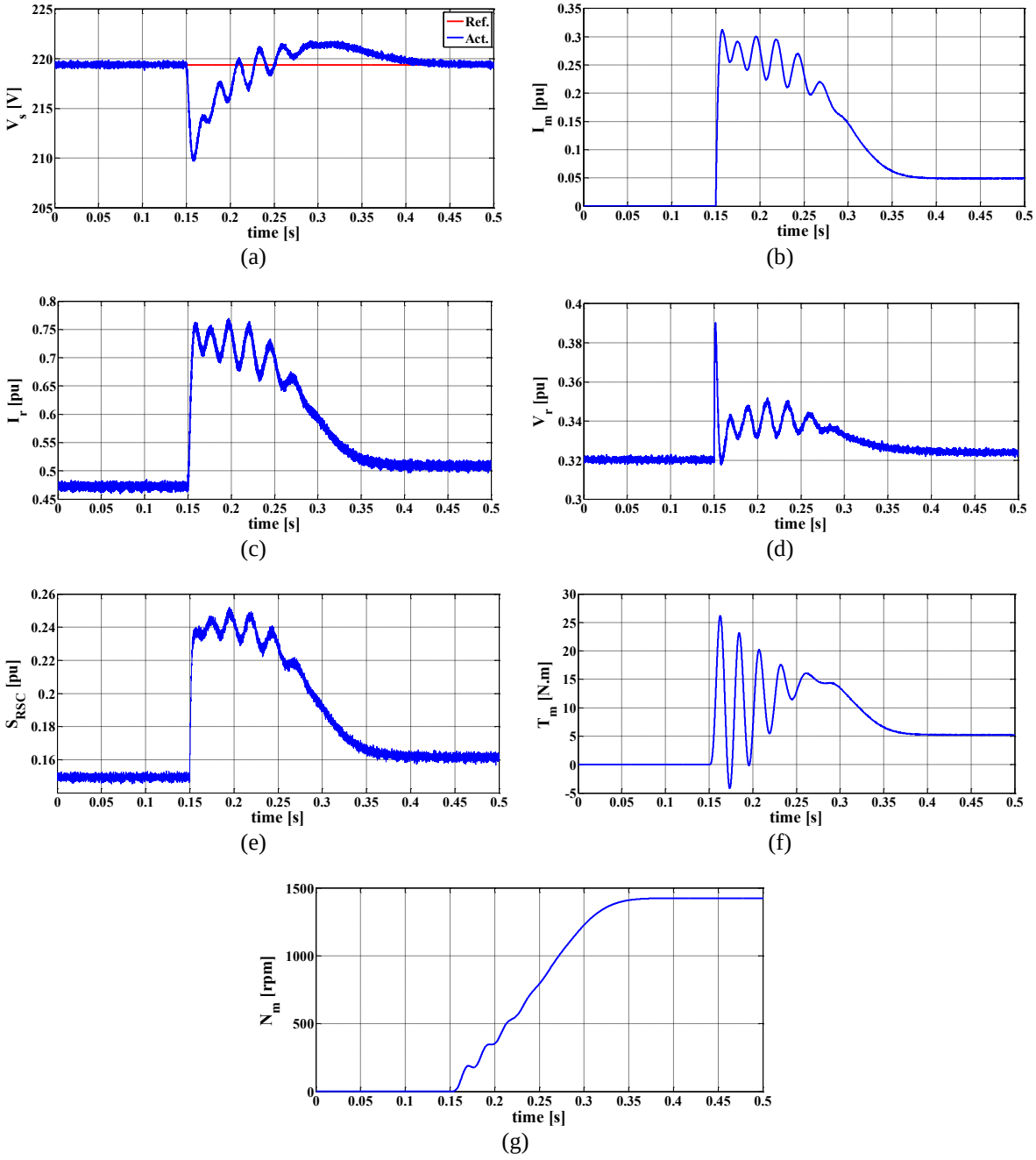

Figure 8. Startingof 1-hp IM at nominal voltage and frequency, (a) stator voltage, (b) IM current, (c) rotor voltage, (d) rotor current, (e) RSC apparent power, (f) motor load torque, and (g) motor speed

5.2. V/f operation

In this section, V/f control method is used to start an IM as it provides good control of starting current [39]–[41]. Several IMs with different hp ratings are connected individually across 15 kW DFIG so that the maximum allowable hp rating is determined using the direct online starting method. The DFIG speed is set at 1050 rpm. The generator speed is held constant during starting and steady state. The DFIG is initially started from t=0 to 0.15 sec. at no-load condition with stator VF outputs equals 80% of the nominal values until it reaches steady state. Next, an IM with hp rating of 1.5 hp is directly connected to the DFIG at t=0.15 sec. At t 0.25 sec., the stator VF outputs are increased gradually until they reach the nominal values of 380 V and 50 Hz. During starting period, the rotor apparent power, voltage, current, and the stator current are recorded in which the power ratings of RSC and DFIG do not overtake the desired limits.

The pervious steps are re-executed by decreasing the starting frequency and increasing the started hp rating of IM every time until reaches to the minimum starting frequency and the maximum started IM hp rating. The results illustrate that the DFIG can be start-up an IM with hp rating of 7.25 hp at a minimum starting frequency about 18.5 Hz without overtaking the desired capacity limits of DFIG and RSC. Figures 9(a) to (h) show the simulation results during start-up and steady state period of 7.25 hp IM [38]. As shown, the rotor voltage is close to its maximum limit of 0.4 pu. Also, the stator current is close to its maximum limit of 1 pu, while the reminder limits still below their maximum limits. Hence, the DFIG cannot start an IM above 7.25 hp as any decreasing of starting frequency or increasing of IM hp rating will cause the rotor voltage and stator current to exceed their limits.

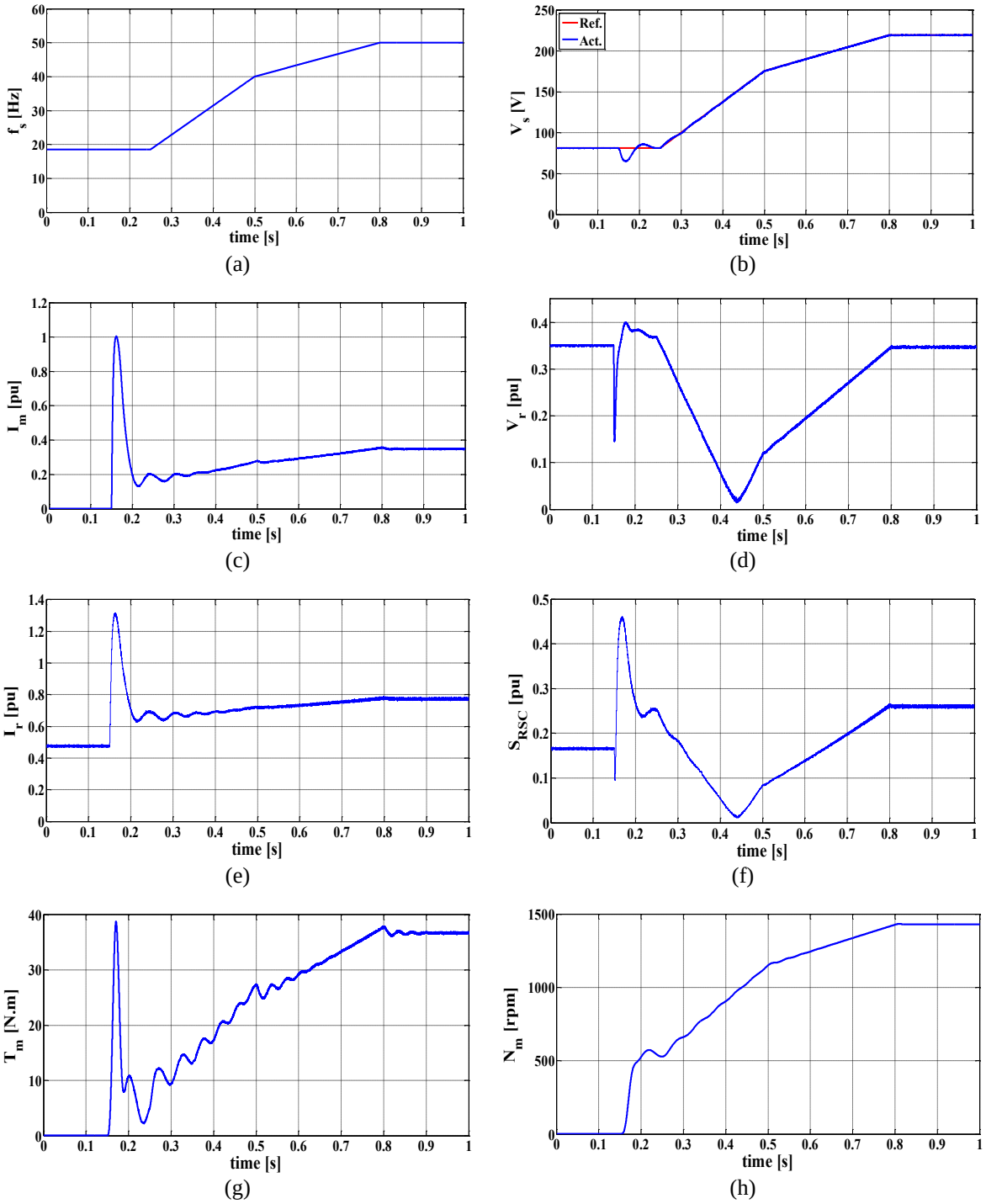

Figure 9. Starting of 7.25-hp IM at using V/f control, (a) stator frequency, (b) stator voltage, (c) IM current, (d) rotor voltage, (e) rotor current, (f) RSC apparent power, (g) motor load torque, and (h) motor speed

6. CONCLUSION

The voltage and frequency of a stand-alone doubly fed induction generator (DFIG) can be controlled irrespective of the generator speed through the rotor input terminals. Adjusting the input rotor frequency yields the required output frequency. Adjusting the magnitude of the injected voltage yields the necessary output voltage. It is proposed in this paper to operate the generator in constant V/f mode to enable a safe starting for a larger-rated induction motor (IM). It is found that the limits of the generator and the rotor-side converter (RSC) depend on the stator frequency and slip. Reducing the output frequency to minimize the start-up current of the motor may exceed the generator limits. Therefore, there is a compromise to find the frequency that ensures the safe starting of the maximum allowable HP rating of a connected IM. A case study is presented in this paper for a 15 kW DFIG. It is found that the generator operates in a constant voltage and frequency mode that can only start motors up to 1 hp. On the other hand, using the proposed technique, it is possible to start larger motors up to 7.25 hp.

ACKNOWLEDGEMENTS

The authors express their gratitude to Benha University, Cairo University, Future University, and Universitas Ahmad Dahlan for their support in conducting this collaborative research. The Embedded Systems and Power Electronics Research Group also provides support for this work.

REFERENCES

[1] F. Abdoune, D. Aouzellag, and K. Ghedamsi, "Terminal voltage build-up and control of a DFIG based stand-alone wind energy conversion system," *Renew. Energy*, vol. 97, pp. 468–480, Nov. 2016, doi: 10.1016/j.renene.2016.06.005.

[2] R. D. Shukla and R. K. Tripathi, "Isolated Wind Power Supply System using Double-fed Induction Generator for remote areas," *Energy Convers. Manag.*, vol. 96, pp. 473–489, May 2015, doi: 10.1016/j.enconman.2015.02.084.

[3] A. A. J. Jeman, N. M. S. Hannoon, N. Hidayat, M. M. H. Adam, I. Musirin, and V. V., "Stability check of doubly fed induction generator (DFIG) micro grid power system," *Bull. Electr. Eng. Informatics*, vol. 8, no. 2, pp. 367–374, Jun. 2019, doi: 10.11591/eei.v8i2.1430.

[4] S. S. Nawaz and S. T. Kalyani, "Reactive power control and performance analysis of doubly fed induction generatorin micro grid," *Indones. J. Electr. Eng. Comput. Sci.*, vol. 28, no. 3, pp. 1214–1226, Dec. 2022, doi: 10.11591/ijeecs.v28.i3.pp1214-1226.

[5] Y. Bakou, M. Abid, L. Saihi, A. G. Aissaoui, and Y. Hammaoui, "Hybrid sliding neural network controller of a direct driven vertical axis wind turbine," *Bull. Electr. Eng. Informatics*, vol. 12, no. 1, pp. 10–20, Feb. 2023, doi: 10.11591/eei.v12i1.4214.

[6] S. Kharoubi and L. El Menzhi, "Wind turbine doubly-fed induction generator defects diagnosis using rotor currents lissajous curves," *Int. J. Power Electron. Drive Syst.*, vol. 11, no. 4, p. 2083, Dec. 2020, doi: 10.11591/ijpeds.v11.i4.pp2083-2090.

[7] C. Ahlem, B. A, D. I, and B. Barkati, "Comparative study of two control strategies proportional integral and fuzzy logic for the control of a doubly fed induction generator dedicated to a wind application," *Int. J. Power Electron. Drive Syst.*, vol. 11, no. 1, p. 263, Mar. 2020, doi: 10.11591/ijpeds.v11.i1.pp263-274.

[8] T. Abdelwahed, M. Radouane, T. Abderrahim, M. Aboulfatah, and R. Nabila, "Comparative study between fast terminal and second order sliding mode controls applied to a wind energy conversion system," *Indones. J. Electr. Eng. Comput. Sci.*, vol. 22, no. 2, p. 765, May 2021, doi: 10.11591/ijeecs.v22.i2.pp765-779.

[9] B. Rached, M. Elharoussi, and E. Abdelmounim, "Hybrid nonlinear control strategies for performance enhancement of a doubly-fed induction aero-generator: design and DSP implementation," *Int. J. Power Electron. Drive Syst.*, vol. 12, no. 3, p. 1472, Sep. 2021, doi: 10.11591/ijpeds.v12.i3.pp1472-1481.

[10] T. Riouch and C. Nichita, "Advanced control strategy of DFIG during symmetrical grid fault," *Int. J. Power Electron. Drive Syst.*, vol. 12, no. 3, p. 1422, Sep. 2021, doi: 10.11591/ijpeds.v12.i3.pp1422-1430.

[11] S. Hassan, B. Abdelmajid, Z. Mourad, S. Aicha, and B. Abdenaceur, "PSO-backstepping controller of a grid connected DFIG based wind turbine," *Int. J. Electr. Comput. Eng.*, vol. 10, no. 1, p. 856, Feb. 2020, doi: 10.11591/ijece.v10i1.pp856-867.

[12] T. Riouch and C. Nichita, "Design and control of DFIG with SMES storage under symmetrical grid fault," *Int. J. Power Electron. Drive Syst.*, vol. 14, no. 1, p. 453, Mar. 2023, doi: 10.11591/ijpeds.v14.i1.pp453-460.

[13] H. M. Seoudy, M. A. Saadeldin, and W. A. Mohamed, "Design and implementation of optimal controller for DFIG-WT using autonomous groups particle swarm optimization," *Int. J. Power Electron. Drive Syst.*, vol. 13, no. 3, p. 1813, Sep. 2022, doi: 10.11591/ijpeds.v13.i3.pp1813-1821.

[14] K. Kouider and A. Bekri, "Small signal stability and dynamic performance investigation on multi-machines power system including DFIG wind farm," *Int. J. Power Electron. Drive Syst.*, vol. 14, no. 3, p. 1825, Sep. 2023, doi: 10.11591/ijpeds.v14.i3.pp1825-1833.

[15] Y. Hocini, A. Allali, and H. M. Boulouiha, "Power fuzzy adaptive control for wind turbine," *Int. J. Electr. Comput. Eng.*, vol. 10, no. 5, p. 5262, Oct. 2020, doi: 10.11591/ijece.v10i5.pp5262-5273.

[16] F.-E. Blouh, B. Boujidi, and M. Bezza, "Wind energy conversion system based on DFIG using three-phase AC-AC matrix converter," *Int. J. Power Electron. Drive Syst.*, vol. 14, no. 3, p. 1865, Sep. 2023, doi: 10.11591/ijpeds.v14.i3.pp1865-1875.

[17] C. Hamid *et al.*, "Performance improvement of the variable speed wind turbine driving a dfig using nonlinear control strategies," *International Journal of Power Electronics and Drive Systems*, vol. 12, no. 4. Institute of Advanced Engineering and Science, pp. 2470–2482, 2021, doi: 10.11591/ijpeds.v12.i4.pp2470-2482.

[18] M. Sharawy, A. A. Shaltout, N. A.- Rahim, M. A. Al-Ahmar, and O. E. M. Youssef, "Starting of induction motor fed with stand-alone DFIG," *Bull. Electr. Eng. Informatics*, vol. 10, no. 5, pp. 2414–2423, Oct. 2021, doi: 10.11591/eei.v10i5.3161.

[19] P. Aree, "Starting performance of induction motor under isolated self-excited induction geneator," in *2015 12th International Conference on Electrical Engineering/Electronics, Computer, Telecommunications and Information Technology (ECTI-CON)*, Jun. 2015, pp. 1–5, doi: 10.1109/ECTICon.2015.7207046.

[20] F. B. Silva, W. E. Vanço, F. A. da S. Gonçalves, C. A. Bissochi, D. P. de Carvalho, and G. C. Guimarães, "A proposal for the

study of voltage sag in isolated synchronous generators caused by induction motor start-up," *Electr. Power Syst. Res.*, vol. 140, pp. 776–785, Nov. 2016, doi: 10.1016/j.epsr.2016.05.008.
[21] M. Falahi, K. L. Butler-Purry, and M. Ehsani, "Induction Motor Starting in Islanded Microgrids," *IEEE Trans. Smart Grid*, vol. 4, no. 3, pp. 1323–1331, Sep. 2013, doi: 10.1109/TSG.2013.2271261.
[22] R. D. Shukla and R. K. Tripathi, "A novel voltage and frequency controller for standalone DFIG based Wind Energy Conversion System," *Renew. Sustain. Energy Rev.*, vol. 37, pp. 69–89, Sep. 2014, doi: 10.1016/j.rser.2014.04.069.
[23] N. K. S. Naidu and B. Singh, "Experimental Implementation of Doubly Fed Induction Generator-Based Standalone Wind Energy Conversion System," *IEEE Trans. Ind. Appl.*, vol. 52, no. 4, pp. 3332–3339, Jul. 2016, doi: 10.1109/TIA.2016.2542783.
[24] B. Singh and S. Sharma, "Doubly fed induction generator-based off-grid wind energy conversion systems feeding dynamic loads," *IET Power Electron.*, vol. 6, no. 9, pp. 1917–1926, Nov. 2013, doi: 10.1049/iet-pel.2013.0010.
[25] J. Nevelsteen and H. Aragon, "Starting of large motors-methods and economics," *IEEE Trans. Ind. Appl.*, vol. 25, no. 6, pp. 1012–1018, 1989, doi: 10.1109/28.44236.
[26] D. Santos-Martin, S. Arnaltes, and J. L. R. Amenedo, "Reactive power capability of doubly fed asynchronous generators," *Electr. Power Syst. Res.*, vol. 78, no. 11, pp. 1837–1840, Nov. 2008, doi: 10.1016/j.epsr.2008.02.007.
[27] S. Engelhardt, I. Erlich, C. Feltes, J. Kretschmann, and F. Shewarega, "Reactive Power Capability of Wind Turbines Based on Doubly Fed Induction Generators," *IEEE Trans. Energy Convers.*, vol. 26, no. 1, pp. 364–372, Mar. 2011, doi: 10.1109/TEC.2010.2081365.
[28] M. Ahmed, M. EL-Shimy, and M. A. Badr, "Advanced modeling and analysis of the loading capability limits of doubly-fed induction generators," *Sustain. Energy Technol. Assessments*, vol. 7, pp. 79–90, Sep. 2014, doi: 10.1016/j.seta.2014.03.002.
[29] S. J. Chapman, *Electric Machinery Fundamentals*. 5th ed., New York, McGraw-Hill, 2012.
[30] A. K. Jain and V. T. Ranganathan, "Wound Rotor Induction Generator With Sensorless Control and Integrated Active Filter for Feeding Nonlinear Loads in a Stand-Alone Grid," *IEEE Trans. Ind. Electron.*, vol. 55, no. 1, pp. 218–228, Jan. 2008, doi: 10.1109/TIE.2007.911196.
[31] G. Abad, J. Lopez, M. Rodriguez, L. Marroyo, and G. Iwanski, "Doubly Fed Induction Machine Modelling and Control for Wind Energy Generation Applications," in *John Wiley & Sons*, 2011.
[32] T. Lund, P. Sørensen, and J. Eek, "Reactive power capability of a wind turbine with doubly fed induction generator," *Wind Energy*, vol. 10, no. 4, pp. 379–394, Jul. 2007, doi: 10.1002/we.228.
[33] M. E. Montilla-D Jesus, D. Santos-Martin, S. Arnaltes, and E. D. Castronuovo, "Optimal Operation of Offshore Wind Farms With Line-Commutated HVDC Link Connection," *IEEE Trans. Energy Convers.*, vol. 25, no. 2, pp. 504–513, Jun. 2010, doi: 10.1109/TEC.2009.2033575.
[34] Z. Chen, J. M. Guerrero, and F. Blaabjerg, "A Review of the State of the Art of Power Electronics for Wind Turbines," *IEEE Trans. Power Electron.*, vol. 24, no. 8, pp. 1859–1875, Aug. 2009, doi: 10.1109/TPEL.2009.2017082.
[35] K. Manickavasagam, "Load Frequency Control of DFIG-isolated and Grid Connected Mode," *Int. J. Appl. Power Eng.*, vol. 1, no. 1, pp. 29–36, 2012, doi: 10.11591/ijape.v1.i1.pp29-36.
[36] R. Datta and V. T. Ranganathan, "Variable-speed wind power generation using doubly fed wound rotor induction machine-a comparison with alternative schemes," *IEEE Trans. Energy Convers.*, vol. 17, no. 3, pp. 414–421, Sep. 2002, doi: 10.1109/TEC.2002.801993.
[37] S. Soued *et al.*, "Experimental behaviour analysis for optimally controlled standalone DFIG system," *IET Electr. Power Appl.*, vol. 13, no. 10, pp. 1462–1473, Oct. 2019, doi: 10.1049/iet-epa.2018.5648.
[38] M. Inc., "MATLAB version: 9.13. 0 (R2022b), Natick, Massachusetts: The MathWorks Inc," 2022.
[39] S. Leng, A. R. N. M. R. Ul Haque, N. Perera, A. Knight, and J. Salmon, "Soft Start and Voltage Control of Induction Motors Using Floating Capacitor H-Bridge Converters," *IEEE Trans. Ind. Appl.*, vol. 52, no. 4, pp. 3115–3123, Jul. 2016, doi: 10.1109/TIA.2016.2539253.
[40] M. Kollipara and V. N. S. R. Kolluru, "Invention into the AC Voltage Regulator with V/F Technique for Induction Motor Starting Applications," *Bull. Electr. Eng. Informatics*, vol. 4, no. 4, pp. 298–303, Dec. 2015, doi: 10.11591/eei.v4i4.513.
[41] S. N. Mahsahirun, N. R. N. Idris, Z. M. Yusof, and T. Sutikno, "Fundamental elements of constant volt/hertz induction motor drives based on dSPACE DS1104 controller," *Int. J. Power Electron. Drive Syst.*, vol. 11, no. 4, pp. 1670–1685, Dec. 2020, doi: 10.11591/ijpeds.v11.i4.pp1670-1685.

BIOGRAPHIES OF AUTHORS

Mohamed Sharawy graduated from Benha University in 2010 and received the M.Sc. degree from Cairo University, Cairo, Egypt, in 2016. In 2021 he received the Ph.D. from the Faculty of Engineering at Shoubra, Cairo, Egypt. His fields of interest include electrical machines, power electronics, control, and renewable energy. He can be contacted at email: mohamed.anwer@feng.bu.edu.eg.

Adel A. Shaltout is a professor at the Department of Electric Power, Cairo University. He obtained his B.Sc. and M.Sc. from Cairo University in 1970 and 1973. He obtained a second M.Sc. from McMaster University and Ph.D. from University of Saskatchewan, Canada. His field of interest includes electrical machines, power systems, and renewable energy sources where he has published more than 190 papers. He is a partner in the Electrical Engineering Consulting Group since 1985 where he has consulted for several industrial firms. He can be contacted at email: aashaltout@yahoo.com.

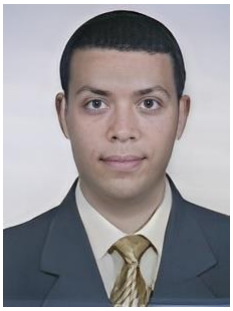

Omar El-Sayed Mohammed Youssef received the B.Sc. and M.Sc. degrees in electrical power and machines from Faculty of Engineering at Shoubra, Benha Branch, Zagazig University, Cairo, Egypt in 1999 and 2004 respectively. He received the Ph.D. degree in Electrical Machines and Electrical Drive Systems from Faculty of Engineering at Shoubra, Benha University, Cairo, Egypt in 2010. He is a Lecturer at the Department of Electrical Engineering, Faculty of Engineering at Shoubra, Benha University. He can be contacted at email: omsamoh@yahoo.com.

Mahmoud A. Al-Ahmar received the B.Sc., M.Sc. and Ph.D. degrees from Faculty of Engineering (Shoubra), Benha University, Cairo/Egypt in 1982, 1987, and 1993, respectively. From 1982 to 1987, he was a demonstrator and Research Assistant with Benha University. In 1993 he became an Assistant professor and in 1999 he became an Associate professor with Benha University. Since 2019 he has been a professor of Electrical Machines at the Faculty of Engineering (Shoubra) of Benha University. He can be contacted at email: ma_alahmar2@hotmail.com.

Naser Abdel-Rahim Ph.D. currently holds the position of Professor in the Department of Electrical Engineering of Future University in Egypt. From 2013 to 2017 he had been a Professor with the Faculty of Engineering at Shoubra, Benha University, Egypt. He received both the M. Eng. and Ph.D. degrees from the Memorial University of Newfoundland in Canada, in 1989 and 1995, respectively. As an Assistant Professor at the United Arab Emirates University (UAEU) from 2000 till 2005, he obtained several research projects funding from the UAEU as well as from Asea Brown Boveri (ABB). Prof. Abdel-Rahim has numerous publications in international journals and refereed conferences, where he also served as a reviewer. He can be contacted at email: naser.abdelrahim@fue.edu.eg.

Tole Sutikno is a lecturer, and serves as the head of the Department of Electrical Engineering, as well as the head of the Master Program of Electrical Engineering within the Faculty of Industrial Technology at Universitas Ahmad Dahlan (UAD) in Yogyakarta, Indonesia. In 1999, 2004, and 2016, he graduated with a Bachelor of Engineering from Universitas Diponegoro, a Master of Engineering from Universitas Gadjah Mada, and a Doctor of Philosophy in Electrical Engineering from Universiti Teknologi Malaysia. All three degrees are in the field of electrical engineering. Since 2023, he has been a Professor at UAD in Yogyakarta, Indonesia, and previously an Associate Professor since 2008. He is among the top 2% of researchers named by Stanford University and Elsevier BV as the most influential scientists in the world for 2021–present. His research interests include the areas of digital design, industrial applications, industrial electronics, industrial informatics, power electronics, motor drives, renewable energy, FPGA applications, embedded systems, artificial intelligence, intelligent control, digital libraries, and information technology. He can be contacted at email: tole@te.uad.ac.id.